MOLECULAR AND CELLULAR BIOLOGY, Aug. 2008, p. 4875–4882 Vol. 28, No. 15
0270-7306/08/$08.00+0 doi:10.1128/MCB.00222-08

Targeted Disruption of the Wnt Regulator Kremen Induces Limb Defects and High Bone Density▽†

Kristina Ellwanger,[1] Hiroaki Saito,[2] Philippe Clément-Lacroix,[3] Nicole Maltry,[1] Joachim Niedermeyer,[1] Woon Kyu Lee,[4]‡ Roland Baron,[2] Georges Rawadi,[3] Heiner Westphal,[4] and Christof Niehrs[1]*

Division of Molecular Embryology, Deutsches Krebsforschungszentrum, DKFZ-ZMBH Alliance, Im Neuenheimer Feld 280, D-69120 Heidelberg, Germany[1]; Harvard University, School of Medicine and School of Dental Medicine, Boston, Massachusetts 02115[2]; Galapagos Company, Romainville, France[3]; and Laboratory of Mammalian Genes and Development, National Institute of Child Health and Human Development, National Institutes of Health, Bethesda, Maryland 20892-2790[4]

Received 11 February 2008/Returned for modification 1 April 2008/Accepted 19 May 2008

Kremen1 and Kremen2 (Krm1 and Krm2) are transmembrane coreceptors for Dickkopf1 (Dkk1), an antagonist of Wnt/β-catenin signaling. The physiological relevance of Kremen proteins in mammals as Wnt modulators is unresolved. We generated and characterized *Krm* mutant mice and found that double mutants show enhanced Wnt signaling accompanied by ectopic postaxial forelimb digits and expanded apical ectodermal ridges. Triple mutant *Krm1*$^{-/-}$ *Krm2*$^{-/-}$ *Dkk1*$^{+/-}$ mice show enhanced growth of ectopic digits, indicating that *Dkk1* and *Krm* genes genetically interact during limb development. Wnt/β-catenin signaling also plays a critical role in bone formation. Single *Krm* mutants show normal bone formation and bone mass, while double mutants show increased bone volume and bone formation parameters. Our study provides the first genetic evidence for a functional interaction of Kremen proteins with Dkk1 as negative regulators of Wnt/β-catenin signaling and reveals that Kremen proteins are not universally required for Dkk1 function.

Wnt proteins and their receptors play important roles in development, differentiation, and disease, and their activity is regulated by a number of transmembrane and extracellular proteins (10, 12, 31, 39). The Wnt coreceptors low-density lipoprotein receptor-related protein 5 and 6 (LRP5 and LRP6) are essential for signal transmission via the β-catenin pathway (20) and are negatively regulated by Dickkopf1 (Dkk1), a member of a small family of secretory proteins (38). Dkk1 binds to LRP6 and thereby acts as a potent Wnt antagonist. In addition, Dkk1 and LRP6 can form a ternary complex with Kremen1 and Kremen2 (Krm1 and Krm2), which are single transmembrane-spanning proteins that are high-affinity receptors for Dkk1 (8, 29, 30) and which also can directly bind to LRP6 (19). The ternary LRP6/Dkk1/Kremen complex is rapidly endocytosed, leading to the inhibition of Wnt/β-catenin signaling (30).

Dkk1 null mutant mice are embryonic lethal. Besides anterior head truncations, they also show fused vertebrae and limb defects (2, 28, 33), which are consistent with the important role of Wnt signaling in regulating the patterning and growth of the vertebrate limb (11). For example, *Wnt3* mutants have a reduced apical ectodermal ridge (AER) (7, 46), a signaling center that controls limb growth. Similarly, the overexpression of *Dkk1* in chicks induces limb truncation, and this is accompanied by apoptosis (18, 33). Conversely, overactivated β-catenin induces the expansion of the AER (46). Expanded AER also is observed in both *Dkk1* null and hypomorphic *Dkk1*$^{d/d}$ mutants, suggesting a genetic interaction with Wnt3 (2, 28, 33). In addition to AER expansion, *Dkk1* null and *Dkk1*$^{d/d}$ mutants display postaxial polysyndactyly in the forelimbs (28, 33). Consistent with the polydactyly in *Dkk1*$^{d/d}$ mice resulting from too-high levels of Wnt signaling, normal digit numbers are restored in *Dkk1*$^{d/d}$ *Lrp6*$^{+/-}$ mice (28). Polydactyly in Dkk1 mutants can be reversed by the simultaneous loss of *Wnt7a* (2). Thus, Dkk1 can control different steps involving Wnt3 or Wnt7a signaling during mouse limb development and digit patterning.

By various mechanisms, Wnt/β-catenin signaling also promotes bone formation, including the renewal of stem cells, osteoblast proliferation, the induction of osteoblastogenesis, and the inhibition of osteoblast and osteocyte apoptosis (17, 24). The N-terminal gain-of-function mutant proteins of LRP5 occurring in patients with high bone mass (e.g., G171V) show reduced affinity to Dkk1. Therefore, high bone mass in these patients likely is due to LRP5 derepression (3, 9). Similarly, *Lrp5*$^{-/-}$ mice show low bone mass due to the reduced proliferation of precursor cells (23). Conversely, mice overexpressing the G171V LRP5 mutant have high bone mass (5). Heterozygous *Dkk1*$^{+/-}$ mice are viable, but they show a strong increase in bone mineral density (32). Thus, Wnt-Lrp5 signaling is under the negative control of Dkk1 to regulate the physiological levels of bone mass.

While the role of Dkk1 in development has been well characterized, the role of its coreceptors Krm1 and Krm2 is less certain. *Kremen* genes are evolutionarily conserved in vertebrates and are differentially expressed during mouse and frog

* Corresponding author. Mailing address: Division of Molecular Embryology, Deutsches Krebsforschungszentrum, Im Neuenheimer Feld 280, D-69120 Heidelberg, Germany. Phone: 49-6221-42-4690. Fax: 49-6221-42-4692. E-mail: niehrs@dkfz.de.

† Supplemental material for this article may be found at http://mcb.asm.org/.

‡ Present address: Department of Laboratory Animal Medicine, College of Medicine, Yonsei University, 134 Sinchon-dong, Seodaemun-gu, Seoul 120-752, South Korea.

▽ Published ahead of print on 27 May 2008.

development (14, 35). *Krm1* is required for thymus epithelium formation in mice by acting as a Wnt inhibitor (40). Antisense morpholino knockdown experiments in *Xenopus laevis* embryos showed that Krm1 and Krm2 function synergistically with Dkk1 in inhibiting Wnt/β-catenin signaling in embryonic head formation (14). Recently, we found that Krm2 can function independently from Dkk proteins during neural crest induction in *Xenopus*. In the absence of Dkk1, Krm1 and Krm2 promote Wnt/β-catenin signaling by binding to LRP6 and enhancing LRP6 protein levels at the plasma membrane (13, 19).

It remains unclear what roles Kremen proteins have during mouse development. A particularly important question is whether there is an absolute requirement for Kremen proteins in Dkk1-mediated Wnt inhibition or whether this interaction is physiologically relevant only in certain tissues. Transgenic *Dkk1* misexpression now is widely used to probe the role of Wnt/β-catenin signaling in the mouse, and a universal requirement for *Krm* would have important consequences for the design and interpretation of such experiments. Furthermore, recently it has been reported that Krm1 acts as a receptor for R-spondins, a family of extracellular Wnt modulators (8). This is a controversial claim, since previous reports indicated that R-spondin acts via LRP6 and Frizzled (37, 49).

To address these questions, we have generated and characterized *Krm1 Krm2* double mutant mice. Our results indicate that *Kremen* genes are negative regulators of Wnt/β-catenin signaling that interact with *Dkk1* during limb development and that are required for normal bone formation. However, *Kremen* genes are not universally required for *Dkk1* function. Furthermore, our results do not support the hypothesis that Kremen proteins mediate R-spondin signaling.

MATERIALS AND METHODS

Animals. Mice were kept according to international standard conditions, and all animal experiments complied with local and international guidelines for the use of experimental animals. *Kremen1* knockout mice were generated by Deltagen, Inc. (San Mateo, CA), using a targeting construct that leads to the deletion of 70 nucleotides in exon 2 of *Krm1* and the insertion of a 6.9-kb internal ribosomal entry site-*lacZ* reporter and neomycin resistance cassette. *Kremen2* null mice were generated by a conventional gene-targeting strategy by replacing sequences of exons 1 to 6 of *Krm2* with a selection cassette. *Krm1 Krm2* double-knockout mice were generated from double heterozygous mice by interbreeding. Triple mutant mice ($Krm1^{-/-}$ $Krm2^{-/-}$ $Dkk1^{+/-}$) were obtained after mating $Krm1^{-/-}$ $Krm2^{-/-}$ mice with $Dkk1^{+/-}$ mice and interbreeding triple heterozygous mice. All mouse lines were maintained and analyzed in CD1 outbred and C57BL/6 congenic genetic backgrounds.

Genotyping. Adults, newborns, and embryos were genotyped by gene-specific triplex PCRs using the following primers (lengths of wild-type-mouse- and knockout mouse-specific PCR products, respectively, are in parentheses). For *Krm1*, primers were K1-p1, 5′-GGCCGCCCAAGATCTAGCAAAACAT-3′; K1-p2, 5′-CCAGAACAGACATGGCTTCCCACCT-3′; and K1-p3, 5′-AGACAAACGCACACCGGCCTTATTC-3′ (214 bp and 377 bp); for *Krm2*, the primers were K2-p1, 5′-AAACCTGGGTGAGGGAGTCT-3′; K2-p2, 5′-AATGGGAAGAGGAGGAGGAA-3′; and K2-p3, 5′-GTTTTCCCAGTCACGACGTT-3′ (370 bp and 452 bp); for *Dkk1*, the primers were D1-p1, 5′-AGAACTAACCCAGCCCCACAGCAGA-3′; D1-p2, 5′-CTCCTCAGGGAAGACAACAAAGCCG-3′; and D1-p3, 5′-GGGTCAACTCCAAGTTCCACCCAAA-3′ (287 bp and 423 bp). Detailed PCR conditions are available upon request.

Immunoprecipitation and Western blotting. Protein extracts were prepared by homogenizing freshly isolated tissue in lysis buffer containing 150 mM NaCl, 20 mM Tris-HCl, pH 7.4, 1% Triton X-100, 5 mM $MgCl_2$, and protease inhibitors (Roche). Lysates were cleared by centrifugation, and equal amounts of total protein from wild-type and knockout mouse tissue were subjected to immunoprecipitation using anti-mouse Krm1 antibody (R&D Systems) and protein G-agarose (Roche) overnight at 4°C. Bound proteins were eluted in Laemmli buffer and analyzed by sodium dodecyl sulfate-polyacrylamide gel electrophoresis and Western blotting.

Cell culture. All cell lines were maintained in Dulbecco's modified essential medium supplemented with 1% L-glutamine, 1% penicillin-streptomycin, 10% fetal calf serum and were grown in 5% CO_2. Mouse Wnt3a-conditioned medium was produced as previously described (15). *Xenopus* Dkk1- and human Rspo3-conditioned media were produced by the transfection of HEK293T cells with pCS2+-X*dkk1* or pCS2+-ΔC-*hRspo3*-flag and the harvesting of medium fractions. Primary mouse embryo fibroblasts (MEFs) were isolated and cultured as previously described (34). For the preparation of primary cells from embryonic day 10.5 (E10.5) whole embryos or adult mouse kidneys, tissues were manually dissociated and incubated in 0.5% trypsin for 5 or 30 min at 37°C. Primary cells were plated in 24-well plates and stimulated for 4 or 6 h with conditioned medium 1 day after plating.

Quantitative real-time PCR. RNA from cells was isolated and transcribed into cDNA using TRIzol and Superscript II reverse transcriptase according to the manufacturer's protocol (Invitrogen). Quantitative real-time PCR was performed with Sybr green and the Roche LightCycler 480 system. Primer sequences for *Axin2* were the following: forward, 5′-GCAGCAGATCCGGGAGGATGAA-3′; and reverse, 5′-GATTGACAGCCGGGGGTCTTGA-3′. Primers for *Actb* were the following: forward, 5′-GACCCAGATCATGTTTGAGACCT-3′; and reverse, 5′-AGGTCCAGACGCAGGATG-3′. Relative *Axin2* expression (*Axin2*/*Actb*) was normalized to that of unstimulated control samples.

Whole-mount in situ hybridization. Whole-mount in situ hybridization was performed according to a protocol adapted from Wilkinson (50). For AER markers, the treatment of the embryos with proteinase K was omitted or reduced to 4 min at 5 μg/ml. RNA probes were transcribed from plasmids containing full-length open reading frames. Where indicated, whole-mount in situ-stained limb buds were paraffin embedded, sectioned (10 μm), and counterstained with eosin according to standard protocols (34).

Skeletal preparations. Adult mouse limbs and E17.5 embryos were skinned, eviscerated, and fixed in 95% ethanol for 3 to 5 days. Cartilage was stained with 0.15 mg/ml Alcian blue (Polyscience) in 80% ethanol, 20% acetic acid for 24 h. After two washes in 95% ethanol, samples were cleared in 1% (wt/vol) potassium hydroxide and then stained for bone with 0.05 mg/ml Alizarin red S (Sigma) in 2% (wt/vol) potassium hydroxide for 2 h. Samples were rinsed in water, further cleared in 2% (wt/vol) potassium hydroxide, and transferred to 100% glycerol.

Bone phenotyping. The bone phenotype was determined for 12-week-old $Dkk1^{+/-}$, $Krm1^{-/-}$, $Krm2^{-/-}$, $Krm1^{-/-}$ $Krm2^{-/-}$, $Krm1^{-/-}$ $Krm2^{-/-}$ $Dkk1^{+/-}$, and wild-type littermate mice. To label bone mineralization fronts, mice were given calcein (20 mg/kg; Sigma, St. Louis, MO) by subcutaneous injections 10 and 3 days before sacrifice. For osteocalcin level measurements, blood was collected on the day of sacrifice. Urinary deoxypyridinoline cross-link levels (D-Pyr) were measured using a colorimetric assay from Pacific Biometrics Inc. (Tampa, FL) and were normalized to the creatinine concentration (measured by a Metra creatinine assay kit [Quidel, San Diego, CA]) to correct for water excretion as described previously (45). The intra-assay coefficient of variation was 3.1 to 4.8%, and the interassay coefficient of variation was 4.3 to 8.4%.

Mouse tibias were recovered from 12-week-old mice following sacrifice and were used for tomodensitometric and histomorphometric analysis. For tomodensitometry, right tibias were fixed overnight in 3.7% formaldehyde in phosphate-buffered saline (PBS), washed in PBS, and then stored in 70% ethanol. Micro-computed tomography (μCT) scans of the metaphyseal region were performed at an isotropic resolution of 9 μm to obtain trabecular bone structural parameters. Using a two- and three-dimensional (2D and 3D) model and a semiautomatic contouring algorithm, we determined three-dimensional bone volume, bone surface, and trabecular thickness. Three-dimensional images were obtained on a Scanco Medical micro-CT scanner (μCT 20; Scanco Medical AG, Bassersdorf, Switzerland). A total of 450 images were obtained from each bone sample using a 512 by 512 matrix, resulting in an isotropic voxel resolution of 18 by 18 by 18 μm^3. Measurements were stored in 3D image arrays with an isotropic voxel size of 9 μm. A constrained 3D Gaussian filter was used to partly suppress the noise in the volumes. The bone tissue was segmented from marrow using a global thresholding procedure. In addition to the visual assessment of structural images, morphometric indices were determined from the microtomographic data sets. Cortical and trabecular bones were separated using a semiautomated contour-tracking algorithm to detect the outer and inner boundaries of the cortex. In trabecular bone, basic structural metrics were measured using direct 3D morphometry (22, 42). For histomorphometry, the fixed samples then were embedded in methylmethacrylate as previously described (43). Four-micrometer sections were stained with von Kossa stain to quantify the structural parameters (i.e., bone volume, trabecular number, and thickness) and with toluidine blue to measure the cellular parameters (i.e., osteoblast and osteoclast numbers). Un-

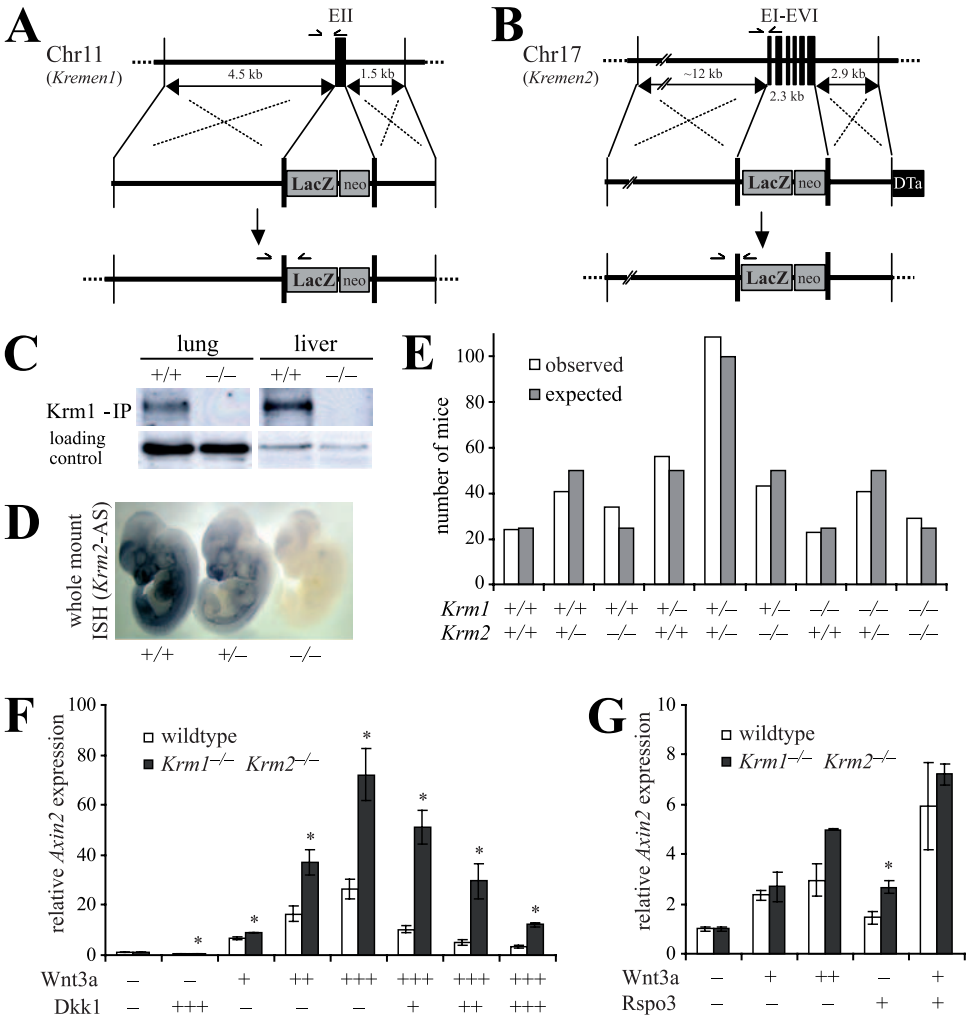

FIG. 1. Targeted mutagenesis indicates that Kremen proteins are not essential mediators of Dkk1 and R-spondin function. (A and B) Diagrams of the *Krm1* (A) and *Krm2* (B) loci, targeting constructs, and knockout alleles after homologous recombination. Targeted exons and homologous sequences are indicated. Small arrows mark positions of primers for triplex PCR genotyping. Diagrams are not drawn to scale. Dta, diphtheria toxin α-subunit; EII, exon 2; EI-VI, exons 1 to 6. (C) Immunoprecipitation and Western blot analysis show the presence of Krm1 protein in wild-type mouse tissue lysates and its absence in $Krm1^{-/-}$ mouse tissue lysates. A cross-reactive band is shown as a loading control. (D) Whole-mount in situ hybridization shows the absence of *Krm2* transcripts in $Krm2^{-/-}$ embryos. (E) Representative genotypic frequencies of 400 mice obtained from crossing mice that were double heterozygous for *Krm1* and *Krm2*. (F and G) Real-time PCR analysis of *Axin2* expression in MEFs (F) or adult kidney cells (G) from wild-type and mutant mice that were treated with the indicated secretion factors (∗, $P < 0.05$).

stained sections were used to assess the dynamic parameters (i.e., bone formation rate and mineral apposition rate). A standard histomorphometric analysis of the tibial metaphysis was performed (41) using the Osteomeasure system (Osteometrics, Inc., Decatur, GA). The measurements were performed in a 1.12-mm^2 area starting 0.3 mm from the proximal growth plate. All histomorphometric measurements were performed in a double-blind fashion, with respect to the treatment regimens, by one individual.

RESULTS AND DISCUSSION

Kremen mutant mice are viable and fertile. We generated constitutive *Krm1* and *Krm2* knockout mice using conventional knockout approaches. In *Krm1* knockout mice, a 70-bp fragment of exon 2 was replaced by a *lacZ* reporter and neomycin resistance cassette (Fig. 1A). In *Krm2* knockout mice, the majority of the protein-coding region was deleted and replaced by a selection cassette (Fig. 1B). To confirm that the targeted alleles are functional null mutations that completely abolish the production of active protein, we performed an immunoprecipitation of Krm1. Western blot analysis showed that a 68-kDa band corresponding to Krm1 is absent in $Krm1^{-/-}$ mouse tissue lysates (Fig. 1C). The absence of *Krm2* transcripts in $Krm2^{-/-}$ tissue was verified by whole-mount in situ hybridization (Fig. 1D) and real-time PCR (not shown).

Since $Krm1^{-/-}$ and $Krm2^{-/-}$ mice were viable and fertile and did not exhibit any obvious abnormalities, we produced *Krm1 Krm2* double knockouts by intercrossing *Krm1* and *Krm2* single mutants. Homozygous $Krm1^{-/-}$ $Krm2^{-/-}$ mice also were viable and fertile and did not exhibit unusual premature mortality. All genotypes produced by intercrossing double heterozygous mice were recovered at the expected Mendelian ratio (Fig. 1E). Also, after intercrossing homozygous mice, normal litter sizes and the normal implantation of embryos in the uterus were observed. These results do not support a re-

cent claim, based on antisense inhibition, that Krm1 functions in embryo implantation and uterine receptivity (25). Furthermore, the requirement of Krm1 and Krm2 in *Xenopus* neural crest development (19) does not seem to be evolutionarily conserved, since no changes in neural crest markers were observed in *Krm* double mutant mice (not shown).

Kremen proteins are not essential mediators of Dkk1 and R-spondin function. We isolated primary cells to analyze if the knockout of *Krm1* and *Krm2* affects the activation of Wnt/β-catenin signaling by Wnt3a or its inhibition by Dkk1. MEFs stimulated with Wnt3a-conditioned medium upregulate the expression of the direct Wnt target gene *Axin2* (Fig. 1F) (21). In two independent $Krm1^{-/-}$ $Krm2^{-/-}$ MEF lines, the Wnt3a-induced upregulation of *Axin2* was elevated compared to that of wild-type cells, supporting the idea that Kremen proteins are negative regulators of Wnt/β-catenin signaling (Fig. 1F and G). Elevated Wnt signaling was not restricted to MEFs but was also found in adult kidney (Fig. 1G) and whole E10.5 embryos (see Fig. S1 in the supplemental material) of mutant mice. However, the treatment of Wnt3a-stimulated MEFs with Dkk1-conditioned medium shows that Dkk1 can efficiently inhibit Wnt/β-catenin signaling despite the absence of *Krm1* and *Krm2* (Fig. 1F).

To test if Kremen proteins are essential mediators for R-spondin/Wnt signaling, we tested primary kidney cells from wild-type and mutant mice. *Axin2* was upregulated by stimulation with either Wnt3a- or Rspo3-conditioned medium in wild-type as well as mutant cells (Fig. 1G), and the treatment of cells with a combination of Rspo3 and Wnt3a further enhanced *Axin2* expression in both genotypes. Our results indicate that the R-spondin-mediated activation of Wnt/β-catenin signaling does not require Kremen proteins. This conclusion also is supported by the fact that R-spondin knockout mouse phenotypes (4, 36) are much more severe than the Kremen double mutant phenotypes (see below). These results do not support the notion that Kremen proteins are essential mediators of R-spondin function (8).

Kremen proteins and Dkk1 interact during limb development. While *Krm1 Krm2* double knockout mice were viable, 74% (n = 140) showed ectopic postaxial forelimb digits (Fig. 2A and B). The size of these ectopic skeletal elements was variable, with approximately half of them being smaller (n = 45/140) and the other half larger (n = 59/140) than the distal phalanx of adjacent digit V. The ectopic digits were outgrowths of digit V rather than originating from the carpus, as regular digits do.

Limb defects similar to those in *Krm* knockouts are found in *Dkk1* mutants (33). We therefore tested for a genetic interaction between *Dkk1* and *Krm1 Krm2* mice by generating triple mutants. While $Dkk1^{+/-}$ mice have normal limbs (Fig. 2B) (33), heterozygosity for *Dkk1* in triple mutant $Krm1^{-/-}$ $Krm2^{-/-}$ $Dkk1^{+/-}$ mice enhanced the frequency and size of ectopic digits. Furthermore, 40% of the extra digits originated at the carpus, like regular digits (Fig. 2A and B), which was never observed in *Krm* knockouts. In contrast to $Dkk1^{-/-}$ embryos, which exhibit polysyndactyly (33), webbing of bone elements was found in neither $Krm1^{-/-}$ $Krm2^{-/-}$ nor $Krm1^{-/-}$ $Krm2^{-/-}$ $Dkk1^{+/-}$ mice.

Kremen proteins and Dkk1 attenuate Wnt signaling in the developing limb to allow normal limb patterning. Consistent

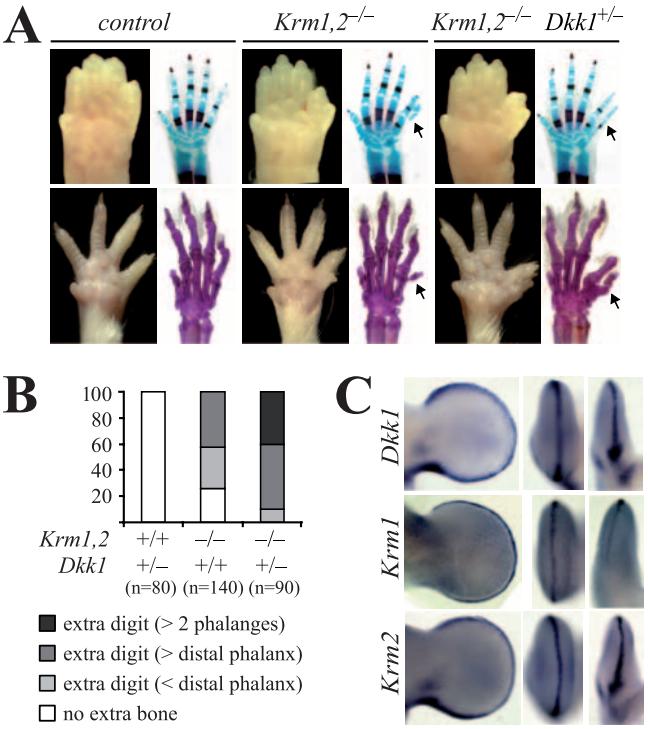

FIG. 2. *Krm1 Krm2* and *Dkk1* functionally interact during forelimb formation. (A) Morphology of embryonic (E17.5) and adult forelimbs in the ventral view. Cartilage and bone were stained with Alcian blue and Alizarin red. Double and triple mutants exhibit postaxial polydactyly (arrows). (B) Statistics of the extra-digit phenotype. (C) Whole-mount in situ hybridization of the indicated genes. Shown are (from left to right) dorsal, frontal, and posterior views of E11.5 forelimbs.

with their role in limb development, *Krm1*, *Krm2*, and *Dkk1* are coexpressed in the AER and also are present at slightly deeper levels in the mesenchyme underlying the AER (Fig. 2C; also see Fig. S2 in the supplemental material). Interestingly, *Dkk1* expression is differentially distributed from distal to more proximal portions of the limb bud. Distally, *Dkk1* expression is restricted to the AER and the adjacent mesenchyme. Proximally, *Dkk1* expression is mesenchymal and vanishes in the ectoderm (see Fig. S2 in the supplemental material). We therefore examined if the knockout of *Krm1 Krm2* affects Wnt signaling in the AER. The expression of *Axin2*, a marker for Wnt/β-catenin signaling (21), is concentrated in the distal AER but is absent from the anterior and posterior margins of the AER in wild-type embryos (Fig. 3A). In $Krm1^{-/-}$ $Krm2^{-/-}$ and $Krm1^{-/-}$ $Krm2^{-/-}$ $Dkk1^{+/-}$ embryos, *Axin2* expression in the forelimb buds clearly was expanded toward more proximal parts of the AER (Fig. 3A). *Axin2* expression was increased in the AER of mutant limbs but not significantly enhanced in the mesenchyme (see Fig. S3A in the supplemental material), consistent with derepressed Wnt/β-catenin signaling in the AER, in which *Kremen* genes and *Dkk1* are coexpressed.

To characterize the molecular consequences of increased Wnt signaling, markers for limb patterning were analyzed. The expression of *Fgf8*, the earliest AER marker and an important regulator of limb growth, clearly was expanded in the posterior limb bud of mutant embryos, the region in which extra digits develop, coinciding with expanded *Axin2* expression (Fig. 3A).

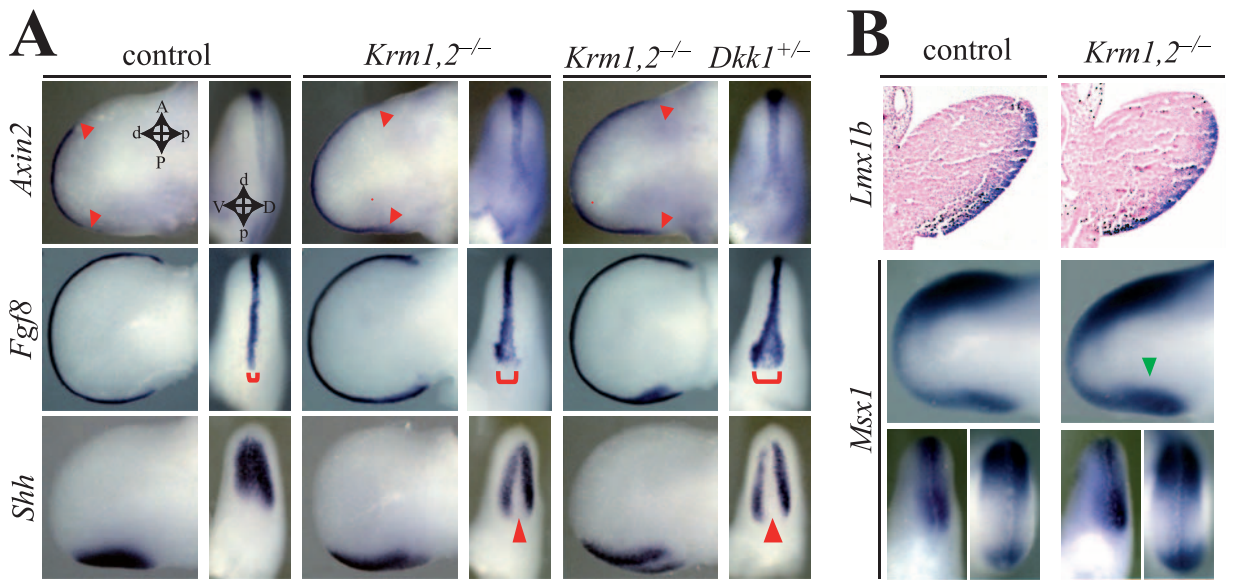

FIG. 3. *Kremen* genes are required for AER patterning. Whole-mount in situ hybridization of marker genes in mutant embryos is indicated. (A) Shown are dorsal and posterior views of E10.5 (*Axin2* and *Shh*) or E11.5 (*Fgf8*) forelimb buds. Red arrowheads in *Axin2* and *Shh* indicate gene expression boundaries and a widening expression gap, respectively. (B) In the upper part, sections from E10.5 forelimbs show the restriction of *Lmx1b* expression to the dorsal side; in the lower part, dorsal, posterior, and frontal views of E10.5 forelimb buds (*Msx1*) are shown. A green arrowhead indicates expanded posterior *Msx1* expression. A, anterior; P, posterior; D, dorsal; V, ventral; d, distal; and p, proximal.

Shh, which is expressed in the posterior mesenchyme complementary to *Fgf8*, was reduced in mutant limbs in the region underlying the expanded AER, leading to a bifurcation of the *Shh* expression domains (Fig. 3A; also see Fig. S3B in the supplemental material).

Unlike with *Axin2*, the expression of *Lmx1b*, a downstream target of Wnt7a signaling, was not altered in the developing limbs of mutant embryos (Fig. 3B). Consistent with this finding, defects in dorsoventral patterning, which is mediated by Wnt7a signaling, were not detected in mutant limbs, suggesting that Krm and Dkk1 specifically regulate limb patterning on the level of Wnt3-mediated AER induction.

The results indicate that Kremen proteins and Dkk1 cooperate as inhibitors of Wnt3/β-catenin signaling during AER induction and maintenance, thereby fine-tuning downstream target gene expression to maintain the normal structure and function of the AER. However, Dkk1 has additional Kremen-independent functions during limb patterning and development. In $Dkk1^{-/-}$ mice, the webbing of digits and the down-regulation of apoptosis mediating *Msx1* is observed (18, 33). In contrast, no syndactyly (Fig. 2A) or decreased *Msx1* expression (Fig. 3B) was observed in limbs of $Krm1^{-/-}$ $Krm2^{-/-}$ or $Krm1^{-/-}$ $Krm2^{-/-}$ $Dkk1^{+/-}$ mice compared to that of the limbs of wild-type mice. Conversely, we observed a slight expansion of the posterior *Msx1* domain in $Krm1^{-/-}$ $Krm2^{-/-}$ limb buds (Fig. 3B). As AER ectoderm-mesenchyme interactions are known to regulate *Msx1* in the murine limb bud (48), this is a likely consequence of posterior AER expansion.

Taken together, our results suggest that Kremen proteins and Dkk1, by inhibiting Wnt signaling, delimit the posterior boundary of the AER. *Krm* loss leads to increased Wnt3/β-catenin signaling and AER expansion. It is well established that AER signaling regulates mesenchymal cell numbers in the nascent limb bud (47) and, ultimately, the number of digit condensations that form. Various limb mutants with expanded AER display polydactyly phenotypes (1, 26, 27), and conversely, when AER and mesenchymal mass are reduced, fewer digits develop. Therefore, the ectopic digit formation in *Krm* mutants is fully in line with these findings.

Kremen proteins regulate bone formation. Human genetic studies have pointed out the critical roles of Wnt/β-catenin signaling in bone metabolism and bone formation (for a review, see reference 6). This motivated us to investigate the bone phenotype of *Kremen* mutants, including $Krm1^{-/-}$, $Krm2^{-/-}$, and $Krm1^{-/-}$ $Krm2^{-/-}$ animals, which we compared to the bone phenotype of *Dkk1* heterozygous animals ($Dkk1^{+/-}$). Furthermore, we assessed whether the deletion of both *Krm1* and *Krm2* in $Dkk1^{+/-}$ ($Krm1^{-/-}$ $Krm2^{-/-}$ $Dkk1^{+/-}$) mice further enhances the high bone mass observed in $Dkk1^{+/-}$ mice (32).

Tibias from 12-week-old animals were analyzed by μCT for bone volume. An analysis of bones from $Krm1^{-/-}$ or $Krm2^{-/-}$ mice showed no difference in bone volume compared to those from wild-type littermates (data not shown), suggesting redundant functions between these two Dkk1 coreceptors in bone tissue. In contrast, the bone volume in $Krm1^{-/-}$ $Krm2^{-/-}$ double mutants was significantly higher than that of wild-type littermates and in both genders (Fig. 4A). As described previously (32), $Dkk1^{+/-}$ mice displayed increased bone volume that was comparable to that observed in $Krm1^{-/-}$ $Krm2^{-/-}$ mice. In addition, the deletion of one allele of *Dkk1* in $Krm1^{-/-}$ $Krm2^{-/-}$ mice ($Krm1^{-/-}$ $Krm2^{-/-}$ $Dkk1^{+/-}$ animals) did not result in a further increase of bone volume (Fig. 4A). Collectively, these data indicate that deleting both *Krm1* and *Krm2* is equipotent to deleting *Dkk1* in increasing bone mass.

To further confirm the increase in bone mass observed in

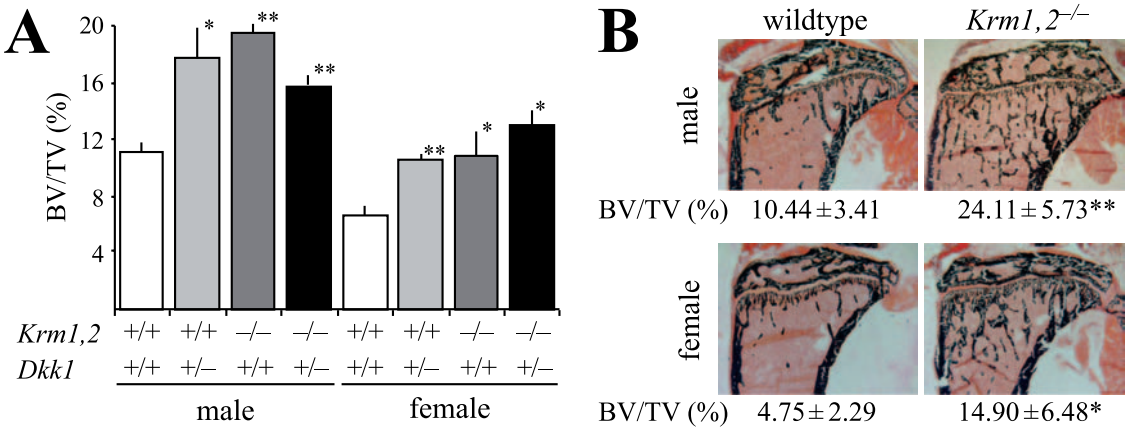

FIG. 4. Knockout of Kremen induces high bone mass. (A) Tomodensitometry analysis of metaphysis tibial bone volume of 12-week-old mice. (B) Photomicrographs of coronal sections through proximal tibias of wild-type and *Krm1*$^{-/-}$ *Krm2*$^{-/-}$ 12-week-old mice stained with von Kossa stain. Note that the number of trabeculae is strongly increased in *Krm1*$^{-/-}$ *Krm2*$^{-/-}$ animals of both genders. The numbers represent the trabecular bone volume of each genotype (*, $P < 0.05$; **, $P < 0.005$). BV, bone volume; TV, total volume.

Krm1$^{-/-}$ *Krm2*$^{-/-}$ mice and to investigate the underlying mechanism, we performed a histomorphometric analysis of the secondary spongiosa in the tibial metaphysis. As shown in Fig. 4B and Table 1, the bone mass of *Krm1*$^{-/-}$ *Krm2*$^{-/-}$ mice was markedly increased compared to that of wild-type mice (Fig. 4B). Trabecular bone volume was significantly elevated in both males and females. While trabecular thickness was unchanged, the number of trabeculae was significantly increased, and trabecular separation was decreased in *Krm1*$^{-/-}$ *Krm2*$^{-/-}$ mice (Table 1). Bone formation parameters all were very significantly elevated in *Krm1*$^{-/-}$ *Krm2*$^{-/-}$ mice, including those for the osteoblast surface, the number of osteoblasts, and the osteoid surface. The dynamic histomorphometry confirmed this marked increase in bone formation, with the mineral apposition rate and the mineralized surface each being increased, leading to a pronounced increase in the bone formation rates (Table 1). The changes observed in both males and females were very similar overall (data not shown).

TABLE 1. Bone structural, cellular, and dynamic parameters of wild-type and *Krm1*$^{-/-}$ *Krm2*$^{-/-}$ male mice

Parameter[a]	Value for indicated mice	
	Wild type	*Krm1*$^{-/-}$ *Krm2*$^{-/-}$[b]
Structural		
BV/TV (%)	10.44 ± 3.41	24.11 ± 5.73**
Trabecular thickness (μm)	46.46 ± 10.17	50.65 ± 9.31
Trabecular separation (μm)	428.23 ± 136.65	163.12 ± 33.98**
No. of trabeculae/mm	2.24 ± 0.62	4.76 ± 0.63**
Cellular		
Osteoid surface/BS (%)	0.90 ± 0.69	4.24 ± 2.23*
Osteoblast surface/BS (%)	6.77 ± 1.32	25.14 ± 6.86**
No. of osteoblasts/μm of BS	2.94 ± 1.91	13.73 ± 3.57**
Eroded surface/BS (%)	1.22 ± 0.55	0.78 ± 0.31
Osteoclast surface/BS (%)	0.70 ± 0.31	0.54 ± 0.20
No. of osteoclasts/mm of BS	0.57 ± 0.21	0.43 ± 0.19
Dynamic		
MS/BS (%)	17.75 ± 4.29	26.23 ± 3.43*
MAR (μm/day)	1.24 ± 0.45	1.81 ± 0.10*
BFR/BS ($\mu m^3/\mu m^2$/day)	83.25 ± 38.62	170.76 ± 25.80**
BFR/BV (%/year)	378.34 ± 177.89	693.50 ± 175.90*
BFR/TV (%/year)	39.97 ± 25.02	159.82 ± 7.78**
D-Pyr (nM)/creatinine (mM)	18.11 ± 1.5	17.08 ± 2.6

[a] Abbreviations: BV, bone volume; TV, total volume; BS, bone surface; MS, mineralized surface; MAR, mineral apposition rate; and BFR, bone formation rate.
[b] *, $P < 0.05$; **, $P < 0.005$.

In contrast to bone formation, there was no significant modification in bone resorption parameters, such as those for the osteoclast surface, the number of osteoclasts, and the eroded surface in *Krm1*$^{-/-}$ *Krm2*$^{-/-}$ male mice (Table 1). In addition, urinary D-Pyr levels were similar in *Krm1*$^{-/-}$ *Krm2*$^{-/-}$ animals and their wild-type littermates, confirming that the loss of Kremen proteins has no impact on bone resorption (Table 1). There was, however, a trend toward a decrease in the histological parameters of bone resorption in males that became statistically significant in females (data not shown). Based on these results, we propose that Kremen proteins and Dkk1 promote bone formation more efficiently than they inhibit bone resorption and osteoclast activity via β-catenin (16).

The results indicate that Kremen proteins are required to negatively regulate bone formation, consistent with their function as Wnt inhibitors. While no enhanced phenotype was observed with *Krm1*$^{-/-}$ *Krm2*$^{-/-}$ *Dkk1*$^{+/-}$ triple mutants, the similarity between the *Krm1 Krm2* null mutant and *Dkk1* heterozygous mutant phenotypes strongly suggests that Kremen proteins function together with Dkk1 in Lrp5 modulation in bone. Our finding that Kremen proteins negatively regulate bone formation may provide new opportunities for therapeutic intervention in, e.g., osteoporosis (6).

In conclusion, *Krm1* and *Krm2* show functional redundancy and are not universally required for *Dkk1* function. *Dkk1* mutants display embryonic lethality, head truncations, and vertebral and limb defects. In contrast, *Kremen* mutants are viable and share only limb defects with *Dkk1* homozygous mice and high bone density with *Dkk1* heterozygous mice. Thus, in many cells, the ability of Dkk1 to prevent Wnt-Lrp6 interaction (44) may be sufficient for effective Wnt antagonism.

ACKNOWLEDGMENTS

We thank C. Cruciat and P. Stannek for sharing reagents, M. Paulsen for critically reading the manuscript, and G. Martin and A. McMahon for providing plasmids for Fgf8 and Shh in situ hybridization probes.

This work was supported by the Deutsche Forschungsgemeinschaft (Ni 286/12-1) and in part by the Intramural Research Program of the NICHD/NIH.

REFERENCES

1. **Adamska, M., B. T. MacDonald, and M. H. Meisler.** 2003. Doubleridge, a mouse mutant with defective compaction of the apical ectodermal ridge and normal dorsal-ventral patterning of the limb. Dev. Biol. **255:**350–362.
2. **Adamska, M., B. T. MacDonald, Z. H. Sarmast, E. R. Oliver, and M. H. Meisler.** 2004. En1 and Wnt7a interact with Dkk1 during limb development in the mouse. Dev. Biol. **272:**134–144.
3. **Ai, M., S. L. Holmen, W. Van Hul, B. O. Williams, and M. L. Warman.** 2005. Reduced affinity to and inhibition by DKK1 form a common mechanism by which high bone mass-associated missense mutations in LRP5 affect canonical Wnt signaling. Mol. Cell. Biol. **25:**4946–4955.
4. **Aoki, M., M. Mieda, T. Ikeda, Y. Hamada, H. Nakamura, and H. Okamoto.** 2007. R-spondin3 is required for mouse placental development. Dev. Biol. **301:**218–226.
5. **Babij, P., W. Zhao, C. Small, Y. Kharode, P. J. Yaworsky, M. L. Bouxsein, P. S. Reddy, P. V. Bodine, J. A. Robinson, B. Bhat, J. Marzolf, R. A. Moran, and F. Bex.** 2003. High bone mass in mice expressing a mutant LRP5 gene. J. Bone Miner. Res. **18:**960–974.
6. **Baron, R., and G. Rawadi.** 2007. Wnt signaling and the regulation of bone mass. Curr. Osteoporos. Rep. **5:**73–80.
7. **Barrow, J. R., K. R. Thomas, O. Boussadia-Zahui, R. Moore, R. Kemler, M. R. Capecchi, and A. P. McMahon.** 2003. Ectodermal Wnt3/beta-catenin signaling is required for the establishment and maintenance of the apical ectodermal ridge. Genes Dev. **17:**394–409.
8. **Binnerts, M. E., K. A. Kim, J. M. Bright, S. M. Patel, K. Tran, M. Zhou, J. M. Leung, Y. Liu, W. E. Lomas, M. Dixon, S. A. Hazell, M. Wagle, W. S. Nie, N. Tomasevic, J. Williams, X. Zhan, M. D. Levy, W. D. Funk, and A. Abo.** 2007. R-Spondin1 regulates Wnt signaling by inhibiting internalization of LRP6. Proc. Natl. Acad. Sci. USA **104:**14700–14705.
9. **Boyden, L. M., J. Mao, J. Belsky, L. Mitzner, A. Farhi, M. A. Mitnick, D. Wu, K. Insogna, and R. P. Lifton.** 2002. High bone density due to a mutation in LDL-receptor-related protein 5. N. Engl. J. Med. **346:**1513–1521.
10. **Cadigan, K. M., and R. M. Nusse.** 1997. Wnt signaling: a common theme in animal development. Genes Dev. **11:**3286–3305.
11. **Church, V. L., and P. Francis-West.** 2002. Wnt signalling during limb development. Int. J. Dev. Biol. **46:**927–936.
12. **Clevers, H.** 2006. Wnt/beta-catenin signaling in development and disease. Cell **127:**469–480.
13. **Cselenyi, C. S., and E. Lee.** 2008. Context-dependent activation or inhibition of Wnt-beta-catenin signaling by Kremen. Sci. Signal **1:**pe10.
14. **Davidson, G., B. Mao, I. Del Barco Barrantes, and C. Niehrs.** 2002. Kremen proteins interact with Dickkopf1 to regulate anteroposterior CNS patterning. Development **129:**5587–5596.
15. **Davidson, G., W. Wu, J. Shen, J. Bilic, U. Fenger, P. Stannek, A. Glinka, and C. Niehrs.** 2005. Casein kinase 1 gamma couples Wnt receptor activation to cytoplasmic signal transduction. Nature **438:**867–872.
16. **Glass, D. A., P. Bialek, J. D. Ahn, M. Starbuck, M. S. Patel, H. Clevers, M. M. Taketo, F. Long, A. P. McMahon, R. A. Lang, and G. Karsenty.** 2005. Canonical Wnt signaling in differentiated osteoblasts controls osteoclast differentiation. Dev. Cell **8:**751–764.
17. **Glass, D. A., and G. Karsenty.** 2006. Molecular bases of the regulation of bone remodeling by the canonical Wnt signaling pathway. Curr. Top. Dev. Biol. **73:**43–84.
18. **Grotewold, L., and U. Rüther.** 2002. The Wnt antagonist Dickkopf-1 is regulated by Bmp signaling and c-Jun and modulates programmed cell death. EMBO J. **21:**966–975.
19. **Hassler, C., C. M. Cruciat, S. Kuriyama, R. Mayor, and C. Niehrs.** 2007. Kremen is required for neural crest induction in Xenopus and promotes LRP6-mediated Wnt signalling. Development **134:**4255–4263.
20. **He, X., M. Semenov, K. Tamai, and X. Zeng.** 2004. LDL receptor related proteins 5 and 6 in Wnt/beta catenin signaling: ARROWS point the way. Development **131:**1663–1677.
21. **Jho, E. H., T. Zhang, C. Domon, C. K. Joo, J. N. Freund, and F. Costantini.** 2002. Wnt/beta-catenin/Tcf signaling induces the transcription of Axin2, a negative regulator of the signaling pathway. Mol. Cell. Biol. **22:**1172–1183.
22. **Kapadia, R. D., G. B. Stroup, A. M. Badger, B. Koller, J. M. Levin, R. W. Coatney, R. A. Dodds, X. Liang, M. W. Lark, and M. Gowen.** 1998. Applications of micro-CT and MR microscopy to study pre-clinical models of osteoporosis and osteoarthritis. Technol. Health Care **6:**361–372.
23. **Kato, M., M. S. Patel, R. Levasseur, I. Lobov, B. H. Chang, D. A. Glass, Jr., C. Hartmann, L. Li, T. H. Hwang, C. F. Brayton, R. A. Lang, G. Karsenty, and L. Chan.** 2002. Cbfa1-independent decrease in osteoblast proliferation, osteopenia, and persistent embryonic eye vascularization in mice deficient in Lrp5, a Wnt coreceptor. J. Cell Biol. **157:**303–314.
24. **Krishnan, V., H. U. Bryant, and O. A. Macdougald.** 2006. Regulation of bone mass by Wnt signaling. J. Clin. Investig. **116:**1202–1209.
25. **Li, J., W. M. Liu, Y. J. Cao, S. Peng, Y. Zhang, and E. K. Duan.** Roles of Dickkopf-1 and its receptor Kremen1 during embryonic implantation in mice. Fertil. Steril., in press.
26. **Loomis, C. A., R. A. Kimmel, C. X. Tong, J. Michaud, and A. L. Joyner.** 1998. Analysis of the genetic pathway leading to formation of ectopic apical ectodermal ridges in mouse Engrailed-1 mutant limbs. Development **125:**1137–1148.
27. **Lu, P., G. Minowada, and G. R. Martin.** 2006. Increasing Fgf4 expression in the mouse limb bud causes polysyndactyly and rescues the skeletal defects that result from loss of Fgf8 function. Development **133:**33–42.
28. **MacDonald, B. T., M. Adamska, and M. H. Meisler.** 2004. Hypomorphic expression of Dkk1 in the doubleridge mouse: dose dependence and compensatory interactions with Lrp6. Development **131:**2543–2552.
29. **Mao, B., and C. Niehrs.** 2003. Kremen2 modulates Dickkopf2 activity during Wnt/LRP6 signaling. Gene **302:**179–183.
30. **Mao, B., W. Wu, G. Davidson, J. Marhold, M. Li, B. Mechler, H. Delius, D. Hoppe, P. Stannek, C. Walter, A. Glinka, and C. Niehrs.** 2002. Kremens are novel Dickkopf receptors that regulate Wnt/beta-catenin signalling. Nature **417:**664–667.
31. **Moon, R. T., A. D. Kohn, G. V. De Ferrari, and A. Kaykas.** 2004. WNT and beta-catenin signalling: diseases and therapies. Nat. Rev. Genet. **5:**691–701.
32. **Morvan, F., K. Boulukos, P. Clement-Lacroix, S. Roman Roman, I. Suc-Royer, B. Vayssiere, P. Ammann, P. Martin, S. Pinho, P. Pognonec, P. Mollat, C. Niehrs, R. Baron, and G. Rawadi.** 2006. Deletion of a single allele of the Dkk1 gene leads to an increase in bone formation and bone mass. J. Bone Miner. Res. **21:**934–945.
33. **Mukhopadhyay, M., S. Shtrom, C. Rodriguez-Esteban, L. Chen, T. Tsukui, L. Gomer, D. W. Dorward, A. Glinka, A. Grinberg, S. P. Huang, C. Niehrs, J. C. Belmonte, and H. Westphal.** 2001. Dickkopf1 is required for embryonic head induction and limb morphogenesis in the mouse. Dev. Cell **1:**423–434.
34. **Nagy, A., M. Gertsenstein, K. Vintersten, and R. Behringer.** 2003. Manipulating the mouse embryo: a laboratory manual. Cold Spring Harbor Laboratory Press, Cold Spring Harbor, NY.
35. **Nakamura, T., S. Aoki, K. Kitajima, T. Takahashi, and K. Matsumoto.** 2001. Molecular cloning and characterization of Kremen, a novel kringle-containing transmembrane protein. Biochim. Biophys. Acta **1518:**63–72.
36. **Nam, J. S., E. Park, T. J. Turcotte, S. Palencia, X. Zhan, J. Lee, K. Yun, W. D. Funk, and J. K. Yoon.** 2007. Mouse R-spondin2 is required for apical ectodermal ridge maintenance in the hindlimb. Dev. Biol. **311:**124–135.
37. **Nam, J. S., T. J. Turcotte, P. F. Smith, S. Choi, and J. K. Yoon.** 2006. Mouse cristin/R-spondin family proteins are novel ligands for the Frizzled 8 and LRP6 receptors and activate beta-catenin-dependent gene expression. J. Biol. Chem. **281:**13247–13257.
38. **Niehrs, C.** 2006. Function and biological roles of the Dickkopf family of Wnt modulators. Oncogene **25:**7469–7481.
39. **Nusse, R.** 2005. Wnt signaling in disease and in development. Cell Res. **15:**28–32.
40. **Osada, M., E. Ito, H. A. Fermin, E. Vazquez-Cintron, T. Venkatesh, R. H. Friedel, and M. Pezzano.** 2006. The Wnt signaling antagonist Kremen1 is required for development of thymic architecture. Clin. Dev. Immunol. **13:**299–319.
41. **Parfitt, A. M., M. K. Drezner, F. H. Glorieux, J. A. Kanis, H. Malluche, P. J. Meunier, S. M. Ott, and R. R. Recker.** 1987. Bone histomorphometry: standardization of nomenclature, symbols, and units. Report of the ASBMR Histomorphometry Nomenclature Committee. J. Bone Miner. Res. **2:**595–610.
42. **Rüegsegger, P., B. Koller, and R. Muller.** 1996. A microtomographic system for the nondestructive evaluation of bone architecture. Calcif. Tissue Int. **58:**24–29.
43. **Sabatakos, G., N. A. Sims, J. Chen, K. Aoki, M. B. Kelz, M. Amling, Y. Bouali, K. Mukhopadhyay, K. Ford, E. J. Nestler, and R. Baron.** 2000. Overexpression of DeltaFosB transcription factor(s) increases bone formation and inhibits adipogenesis. Nat. Med. **6:**985–990.
44. **Semënov, M. V., K. Tamai, B. K. Brott, M. Kuhl, S. Sokol, and X. He.** 2001. Head inducer Dickkopf-1 is a ligand for Wnt coreceptor LRP6. Curr. Biol. **11:**951–961.
45. **Sims, N. A., P. Clement-Lacroix, D. Minet, C. Fraslon-Vanhulle, M. Gaillard-Kelly, M. Resche-Rigon, and R. Baron.** 2003. A functional androgen receptor is not sufficient to allow estradiol to protect bone after gonadectomy in stradiol receptor-deficient mice. J. Clin. Investig. **111:**1319–1327.
46. **Soshnikova, N., D. Zechner, J. Huelsken, Y. Mishina, R. R. Behringer,**

M. M. Taketo, E. B. Crenshaw III, and W. Birchmeier. 2003. Genetic interaction between Wnt/beta-catenin and BMP receptor signaling during formation of the AER and the dorsal-ventral axis in the limb. Genes Dev. **17:**1963–1968.
47. **Sun, X., F. V. Mariani, and G. R. Martin.** 2002. Functions of FGF signalling from the apical ectodermal ridge in limb development. Nature **418:**501–508.
48. **Wang, Y., and D. Sassoon.** 1995. Ectoderm-mesenchyme and mesenchyme-mesenchyme interactions regulate Msx-1 expression and cellular differentiation in the murine limb bud. Dev. Biol. **168:**374–382.
49. **Wei, Q., C. Yokota, M. V. Semenov, B. Doble, J. Woodgett, and X. He.** 2007. R-spondin1 is a high affinity ligand for LRP6 and induces LRP6 phosphorylation and beta-catenin signaling. J. Biol. Chem. **282:**15903–15911.
50. **Wilkinson, D. G.** 1992. In situ hybridisation. A practical approach. Oxford University Press, Oxford, United Kingdom.